Stabilization of Sulfide Radical Cations through Complexation with the Peptide Bond: Mechanisms Relevant to Oxidation of Proteins Containing Multiple Methionine Residues

Krzysztof Bobrowski,[†] Gordon L. Hug,*[,‡,§,||] Dariusz Pogocki,[†,⊥] Bronislaw Marciniak,[§] and Christian Schöneich[⊗]

Institute of Nuclear Chemistry and Technology, 03-195 Warsaw, Poland, Radiation Laboratory, University of Notre Dame, Notre Dame, Indiana 46556, Faculty of Chemistry, Adam Mickiewicz University, 60-780 Poznan, Poland, Faculty of Chemistry, Rzeszow University of Technology, 35-959 Rzeszow, Poland, and Department of Pharmaceutical Chemistry, University of Kansas, Lawrence, Kansas 66047.

Received: February 12, 2007; In Final Form: May 31, 2007

The recent study on the •OH-induced oxidation of calmodulin, a regulatory "calcium sensor" protein containing nine methionine (Met) residues, has supported the first experimental evidence in a protein for the formation of S∴N three-electron bonded radical complexes involving the sulfur atom of a methionine residue and the amide groups in adjacent peptide bonds. To characterize reactions of oxidized methionine residues in proteins containing multiple methionine residues in more detail, in the current study, a small model cyclic dipeptide, *c*-(L-Met−L-Met), was oxidized by •OH radicals generated via pulse radiolysis and the ensuing reactive intermediates were monitored by time-resolved UV−vis spectroscopic and conductometric techniques. The picture that emerges from this investigation shows there is an efficient formation of the Met(S∴N) radicals, in spite of the close proximity of two sulfur atoms, located in the side chains of methionine residues, and in spite of the close proximity of sulfur atoms and oxygen atoms, located in the peptide bonds. Moreover, it is shown, for the first time, that the formation of Met(S∴N) radicals can proceed directly, via H^+-transfer, with the involvement of hydrogen from the peptide bond to an intermediary hydroxysulfuranyl radical. Ultimately, the Met(S∴N) radicals decayed via two different pH-dependent reaction pathways, (i) conversion into sulfur−sulfur, intramolecular, three-electron-bonded radical cations and (ii) a proposed hydrolytic cleavage of the protonated form of the intramolecular, three-electron-bonded radicals {Met(S∴N)/Met(S∴NH)$^+$} followed by electron transfer and decarboxylation. Surprisingly, also α-(alkylthio)alkyl radicals enter the latter mechanism in a pH-dependent manner. Density functional theory computations were performed on the model *c*-(L-Met−Gly) and its radicals in order to obtain optimizations and energies to aid in the interpretation of the experiments on *c*-(L-Met−L-Met).

Introduction

Sulfide radical cations have recently attracted considerable attention. In particular they are implicated in assorted biological electron transfers where sulfide radical cations are likely intermediates in biological redox processes.[1−7] There is unambiguous theoretical[2,8−13] and experimental evidence[14−40] that sulfide radical cations (>$S^{+\bullet}$) can be stabilized through intramolecular complexation with Lewis bases (nucleophiles) that are present in neighboring groups, see the reaction in eq 1 where Y represents the heteroatoms S, Se, Te, O, N, P, Cl, Br, or I, and L represents an organic ligand and/or H ($m = 0-2$; $n = 0, 1$):

$$R_2S^{+\bullet} + (YL_m)^{n-} \rightarrow [R_2S\therefore YL_m]^{(1-n)+} \qquad (1)$$

These neighboring groups generally act by providing electron lone pairs that can stabilize sulfide radical cations through the overlap of the heteroatoms' doubly occupied p orbitals with the singly occupied p orbital of the sulfur. The resulting bond is a three-electron bond of the type $2\sigma/1\sigma^*$.

Reactions of this type are of special interest to biology and medicine when stabilization of sulfide radical cations occurs in peptides and proteins.[1,41] There is increasing evidence that methionine sulfide radical cations, Met($S^{+\bullet}$), are involved in oxidative damage to peptides and proteins. The methionine (Met) residues in these biopolymers are susceptible to attack by reactive oxygen species (ROS) during oxidative stress and biological aging.[41−44] Moreover, the pathogenesis of some neurodegenerative diseases (Alzheimer's, Jacob−Creutzfeld's, and Parkinson's) seems to be strongly linked to the presence in brain tissue of β-amyloid peptide (βAP),[45] human prion protein (hPrP), and an aggregated form of α-synuclein,[46] respectively. These macromolecules contain several mechanistically important methionine(s) such as Met[35] in the C-terminal α-helical domain of βAP,[47] Met[205], Met[206], and Met[213] within the α-helical segments of hPrP,[48] and four Met residues in α-synuclein.[46−48]

Frequently heteroatoms in peptide bonds are the only nucleophiles present in the vicinity of Met($S^{+\bullet}$). In this regard, it was recently shown that such interactions play an important role in oligopeptides of the form *N*-Ac-GMG and *N*-Ac-GGGMGGG. Intramolecularly bonded sulfide radical cations,

* Corresponding author. Gordon L. Hug, Radiation Laboratory, University of Notre Dame, Notre Dame, Indiana 46556. Fax: (001-574)-631-8068. E-mail: hug.1@nd.edu.

[†] Institute of Nuclear Chemistry and Technology.

[‡] University of Notre Dame.

[§] Adam Mickiewicz University.

[||] Fullbright scholar in the Faculty of Chemistry, Adam Mickiewicz University. Permanent address: Radiation Laboratory, University of Notre Dame.

[⊥] Rzeszow University.

[⊗] University of Kansas.

10.1021/jp071191w CCC: $37.00
Published on Web 07/21/2007

Met($S^{+\bullet}$), were directly observed in these systems with the bonding partner being either the carbonyl oxygen or the amide nitrogen of a peptide bond.[49] Stabilization of sulfide radical cations through formation of sulfur−oxygen three-electron-bonded radicals might potentially facilitate oxidation and autoxidation processes of Met in peptides and proteins. For instance, the electrochemical oxidation of organic sulfides revealed lower oxidation potentials for those sulfides containing neighboring carboxylate and hydroxy groups compared to unsubstituted sulfides.[50] The first experimental evidence that Met^{35} in β-AP1-42 is more easily oxidized than in other peptides and proteins comes from the one-electron oxidation of βAP1-40 using azide radicals ($N_3^{\bullet}$) produced by pulse radiolysis.[51]

The progress of these free-radical reactions in real biological systems is difficult to unravel in vivo because of the complexity of the chemical environment and the availability of the biological material. In order to define the potential reactions of Met($S^{+\bullet}$) in long oligopeptides and proteins containing multiple and adjacent Met residues (e.g., prion proteins PrP, calmodulin CaM), an attempt has been made in the present work to isolate some of the mechanistic steps during $^{\bullet}$OH-induced oxidation of a cyclic dipeptide (L-Met−L-Met). Cyclic dipeptides are suitable model compounds for the study of peptide free radical chemistry. While appearing very small to be models for proteins, they have the unique feature of having no terminal groups. This makes them invaluable for studying interactions between side chains and peptide bonds. The cyclic L-Met−L-Met peptide itself has been previously studied in some detail.[52] It was shown that $^{\bullet}$OH radicals generate intramolecular (S∴S)-bonded radical cations, cyclo-Met−Met$(S\therefore S)^+$. Moreover, the existence of at least two different precursors of the cyclo-Met−Met$(S\therefore S)^+$ cation was inferred.

In the present study, we identified, characterized, and quantified two complexed sulfide radicals from cyclic L-Met−L-Met: the intramolecular sulfur−nitrogen three-electron-bonded radical Met(S∴N) and the intramolecular sulfur−sulfur three-electron-bonded radical cation Met$(S\therefore S)^+$. These radicals were monitored using time-resolved optical spectroscopy and conductivity. Such information is important for establishing whether, and to what extent, $^{\bullet}$OH-induced oxidation of Met to Met($S^{+\bullet}$) is assisted by the peptide bond in the backbone of proteins containing multiple and proximate methionine residues. We also identified reaction pathways for the pH dependent decay of the intramolecular sulfur−nitrogen three-electron-bonded radical Met(S∴N) and α-(alkylthio)alkyl radicals.

To assist in the interpretation of the data, we performed DFT computations for optimizations and energy calculations of the parent molecules *c*-(L-Met−L-Met) and its simplified model *c*-(L-Met−Gly). Therefore, in the radicals derived from *c*-(L-Met−Gly), one of the Met side chains is replaced by a hydrogen atom and the other Met side chain contains a Met-$(S\therefore O)^+$ radical cation, a Met$(S\therefore NH)^+$, or a Met(S∴N) radical derived from the Met side chain. Moreover, Gibbs free energies of deprotonation at the nitrogen atom of the amide functionality were calculated for *c*-(Gly−Gly), *c*-(L-Ala−L-Ala), and *N*-methylacetamide.

Experimental Section

Materials and Methods: Chemicals. Cyclic L-methionyl−L-methionine peptide, *c*-(L-Met−L-Met), was purchased from Bachem and was used as received. The other chemicals were obtained as follows: perchloric acid ($HClO_4$) was purchased from Aldrich Chemical Co. (Milwaukee, WI) and reagent grade NaOH was obtained from J. T. Baker.

Preparation of Solutions. All solutions were made with deionized water purified in a reverse osmosis/deionization system from ServA-Pure Co. The solutions contained only 0.2 mM of *c*-(L-Met−L-Met) in order to avoid complications connected with the formation of intermolecular S∴S-bonded dimeric radical cations. There was an UV irradiation unit in the circulating section of this water-purification system. The water had a resistance >18 Ω/cm and a total organic carbon (TOC) content of <10 ppb. The pH was adjusted by the addition of either NaOH or $HClO_4$. Solutions were subsequently purged for at least 30 min per 500 mL of sample with the desired gas (N_2O or N_2) before pulse irradiation.

Radiolysis of Water. Pulse irradiation of neutral water leads to the formation of three primary, highly reactive transients shown in the reaction in eq 2. In addition, stable products, H_2, H_2O_2, and H_3O^+ are formed.[53] In N_2O-saturated solutions ($[N_2O]_{sat} \approx 2 \times 10^{-2}$ M),[54] the hydrated electrons, e_{aq}^-, are converted into $^{\bullet}$OH radicals according to the reaction in eq 3 ($k_3 = 9.1 \times 10^9$ M^{-1} s^{-1}).[54] Reaction 3 nearly doubles the amount of $^{\bullet}$OH radicals available for reactions with substrates.

$$H_2O \rightarrow {}^{\bullet}OH, e_{aq}^-, {}^{\bullet}H \quad (2)$$

$$e_{aq}^- + N_2O \rightarrow O^{\bullet-} + N_2\ (+H_2O) \rightarrow {}^{\bullet}OH + OH^- + N_2 \quad (3)$$

The effective radiation chemical yields, *G*, of the primary species, available for the reaction with a substrate, depend on the concentration of the added substrate. For N_2O-saturated solutions, the effective radiation chemical yield of $^{\bullet}$OH radicals, converting a given substrate into substrate-derived radicals, can be calculated on the basis of the formula given by Schuler et al.[55] This formula relates the *G* value of substrate radicals to the product k_s[S], the rate constant, k_s, for the reaction of $^{\bullet}$OH radicals with the substrate times the substrate concentration, [S], itself.

Pulse Radiolysis. Pulse radiolysis experiments were performed with the Notre Dame Titan 8 MeV Beta model TBS 8/16-1S linear accelerator with typical pulse lengths of 2−10 ns. The data acquisition system allows for kinetic traces to be displayed on multiple time scales. A detailed description of the experimental setup for optical measurements has been given elsewhere along with the basic details of the equipment and the data collection system.[56] Absorbed doses per pulse were on the order of 4−8 Gy (1 Gy = 1 J kg^{-1}). For time-resolved measurements of optical spectra, N_2O-saturated solutions containing 10^{-2} M KSCN were used as the dosimeter, with a radiation chemical yield of $G = 0.635$ μmol J^{-1} and a molar absorption coefficient of 7580 M^{-1} cm^{-1} at 472 nm for the $(SCN)_2^{\bullet-}$ radical.[54] The SI units (μmol J^{-1}) for radiation chemical yield, *G*, are the concentration of radicals (in micromoles) produced per joule of energy absorbed.

For time-resolved conductivity measurements, the conductivity apparatus was used which allows high-precision conductometric measurements over a pH range from 3 to 6. (Saturation of the apparatus occurs with lower pH due to the large conductivity, and basic pH should be feasible up to about pH 10, but this has no be thoroughly investigated on the current apparatus to date.) In the current experiments, the pH range was restricted to 4.0−5.5. Above 5.5, the overall dynamics of establishing proton equilibration is too slow to allow investigations of the times scale much below 10 μs. A detailed description of the conductivity apparatus along with the measuring cell has been given elsewhere.[57] The dosimetry was achieved using acidic, aqueous solutions saturated with CH_3Cl and, alterna-

tively, using aqueous solutions saturated with N_2O containing dimethyl sulfoxide. In the first dosimeter system, pulse irradiation yields H^+ and Cl^- with $G(H^+) = G(Cl^-) = 0.285$ μmol J^{-1}, according to reactions in eqs 2 and 4. The respective equivalent conductivities at 18 °C were taken as $\Lambda(H^+) = 315$ S cm^2 equiv^{-1} and $\Lambda(Cl^-) = 65$ S cm^2 equiv^{-1}.[58] In the second

$$e_{aq}^- + CH_3Cl \rightarrow CH_3^\bullet + Cl^- \qquad (4)$$

dosimeter system, pulse irradiation leads to the formation of sulfinic acid according to reactions in eqs 2 and 5. At pH > 3.5, sulfinic acid is completely dissociated. The respective equivalent conductivities at 18 °C were taken as $\Lambda(H^+) = 315$ S cm^2 equiv^{-1} and $\Lambda(MeSO_2^-) = 42$ S cm^2 equiv^{-1}.[59] Radiation

$$^\bullet OH + (H_3C)_2SO \rightarrow H_3C^\bullet + H_3C{-}SO_2^- + H^+ \qquad (5)$$

chemical yields of ions, G(ions), are given in SI units, and their uncertainties are reported as one standard deviation, based on five or more separate pairs of traces. These pairs of traces (one of positive polarity and one of negative polarity) are averaged, taking into account the signs.

All experiments were performed with a continuous flow of sample solutions at room temperature (~20 °C). Experimental error limits are ±10% unless specifically noted.

Resolution of Time-Resolved Optical Spectra. Optical spectra, monitored at various time delays following the electron pulse, were resolved into specific components (representing individual transients) by linear regression according to eq 6.[60]

$$G\epsilon(\lambda_j) = \sum_{i=1}^{n} G_i\epsilon_i(\lambda_j) \qquad (6)$$

Here, $G\epsilon(\lambda_j)$ is equal to the observed absorbance change $\Delta A(\lambda_j)$ of the composite spectrum multiplied by the factor (F) from the dosimetry. $F = \epsilon_{472}G((SCN)_2^{\bullet-})/\Delta A_{472}$, where ϵ_{472} is the molar absorption coefficient of $(SCN)_2^{\bullet-}$ at 472 nm, $G((SCN)_2^{\bullet-})$ is the radiation chemical yield of the $(SCN)_2^{\bullet-}$ radicals, and ΔA_{472} represents the observed absorbance change at 472 nm in the thiocyanate dosimeter. G_i is the linear regression coefficient of the ith species, and $\epsilon_i(\lambda_j)$ is the molar absorption coefficient of the ith species at the jth wavelength. Further details of this method have been described elsewhere.[61] In the following, the listed uncertainties in the G_i's are equal to the square root of the corresponding ith diagonal elements of the covariance matrix from each linear regression.

Several criteria were applied to validate the spectral resolutions and to eliminate unreasonable fits. (i) Within ±15%, the combined yields of the transient species derived from their respective molar absorption coefficients cannot exceed the initial radiation chemical yield of the primary species, i.e., $G_i(H^\bullet + {}^\bullet OH) = 0.62$ μmol J^{-1}. The error limit of ±15% allows for a ±5% variation in the experimental data and a ±10% combined error in the reported molar absorption coefficients for the UV spectra of the components under consideration. (ii) Wherever experimentally measurable, the formation of (radical) ions must be accompanied by a concomitant change of equivalent conductivity. (iii) The radiation chemical yields of the respective species (Chart 1) in the optical spectra were calculated taking the following representative molar absorption coefficients: ϵ_{340}(**1**) = 3400 M^{-1} cm^{-1},[62] ϵ_{510}(**3**) = 6200 M^{-1} cm^{-1},[52] ϵ_{390}(**4**) = 4500 M^{-1} cm^{-1},[63] ϵ_{290}(**5a/5b**) = 3000 M^{-1} cm^{-1},[64] ϵ_{400}(**6**) = 3000 M^{-1} cm^{-1},[21] ϵ_{270}(**7**) = 6250 M^{-1} cm^{-1}, and ϵ_{370}(**7**) = 1800 M^{-1} cm^{-1}.[65] Since two of the species (**4** and **6**) have similar optical-absorption shapes, this procedure will not be reliable, as written in eq 6, in separating two such species. These two radicals can be distinguished by the conductivity measurements since **4** is nonconducting and **6** is conducting. To do this in a systematic, mathematical fashion, the square $|G(\text{ions}) - G(\mathbf{3} + \mathbf{6})|^2$ of the difference between the experimental value, G(ions), and the sum, $G(\mathbf{3} + \mathbf{6})$, of the two fitting parameters was included as an additional term in the linear least-squares summation. However, in any time window, at any particular pH, there is only a single measured value of G(ions), compared to over 30 $\Delta A(\lambda_j)$ values in a typical transient absorption. To put the optical and conductivity measurements on an equal footing, the single conductivity term in the least-squares procedure was weighted by 35.[66]

CHART 1

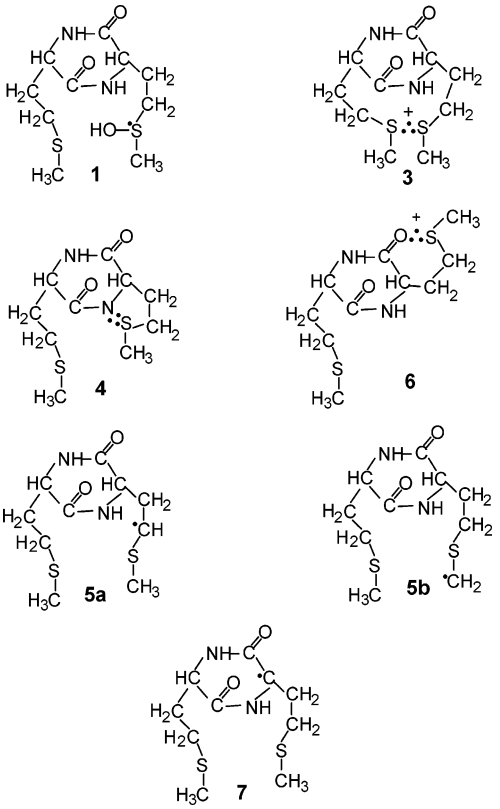

Limitations during Interpretation of Time-Resolved Conductometric Data. Since protons are formed during water radiolysis with $G(H_3O^+) = 0.27$ μmol J^{-1}, conductivity experiments at pH values larger than 5 are difficult to interpret at short time scales due to the slow overall proton equilibration (including protonation of $O^{\bullet-}$ by water in N_2O-saturated aqueous solutions, reaction in eq 3) at such pH values. These limitations have been experimentally validated through pulse irradiation of N_2O-saturated water at the defined pH value, i.e., 5.3.

Computational Methods. Ab initio calculations were performed with the Gaussian 03 suite of quantum chemistry programs.[67] A nonlocal hybrid functional, Becke3LYP, was used.[68] It is commonly applied both to closed and open shell systems. This method appears to be particularly useful for the computation of optimized molecular geometries and properties of radical species, among them species containing thioether functionalities.[2−4,6,8,9,11,12,69] However, since the reliability of the B3LYP functional for three-electron-bonded species has been sporadically contested, the alternative gas-phase calculations were performed applying another nonlocal hybrid functional (BHHLYP) and using Møller−Plesset (MP2) perturbation theory,

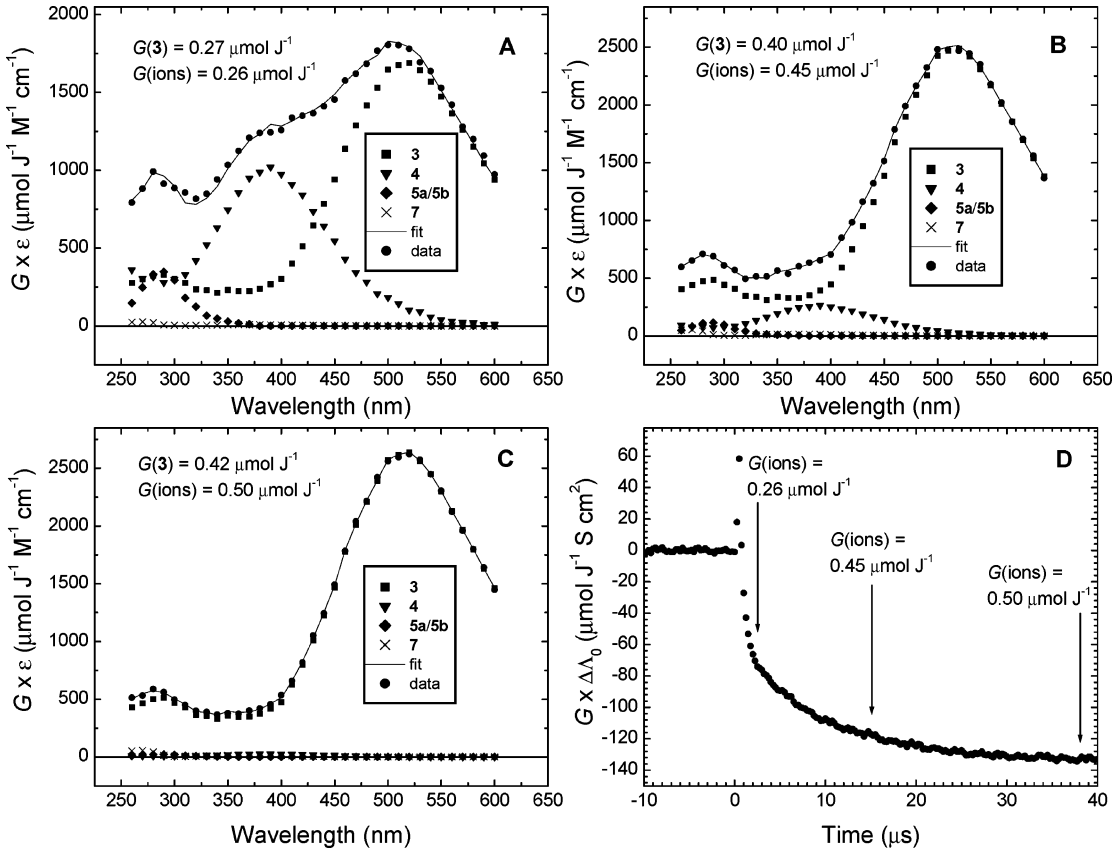

Figure 1. Resolution of the spectral components in the transient absorption spectra taken (A) 2 μs, (B) 15 μs, (C) 37.5 μs after the pulse and (D) equivalent conductivity changes represented as $G\Delta\Lambda$ vs time profile following the •OH-induced oxidation of *c*-(L-Met−L-Met) (2×10^{-4} M) in N_2O-saturated aqueous solutions at pH 4.3.

both previously successfully applied for these kind of radical species.[11,70−72]

Geometry optimization and energy calculations were carried out using the standard 6-31G(d) basis set. This basis set offers a reasonable compromise between the proper description of the species and good performance at a modest computational cost.[73−75] All structures were fully optimized using the analytical gradient technique, and the nature of each identified stationary point was checked by evaluating harmonic frequencies. Vibrational frequencies (ω) obtained from conventional harmonic normal-mode analysis of the respective geometries were used without any corrections. In order to account for the effect of solvent, the Gibbs free energy of solvation was calculated for the gas-phase B3LYP/6-31G(d) geometries of radicals applying the integral equation formalism model (IEFPCM).[76−78] The Gibbs free energies of the two model cyclic peptides *c*-(Gly−Gly) and *c*-(L-Ala−L-Ala), *N*-methylacetamide, and their structures with deprotonated amide functionalities were calculated by applying the Gaussian-3/DFT theory.[79,80] In order to confirm our spectral assignments, theoretical estimates were obtained from time-dependent-density functional response theory (TD-DFRT).[81,82] Estimates were made of both the location of the dominant absorption bands (λ_{max}) and approximate descriptions of their intensities, i.e., their electronic oscillator strength, *f*, and their electronic composition of the transitions. The TD-DFRT-B3LYP/6-311+G(d,p) calculations were done at the geometries obtained in the gas-phase, and the IEFPCM calculations were done on the B3LYP/6-31G(d) level. More details of the computational methods are presented in Supporting Information.

Results

Time-Resolved Optical Absorpton Spectra at pH 4.3. In order to validate the resolutions of the optical spectra, concomitant changes in the samples' equivalent conductivities (vide infra) were followed. At early times, following the radiolysis pulse, the interpretation of these experiments was complicated by the proton relaxation back to the water equilibrium. Thus, the earliest time delay at which spectral resolutions were performed were for the optical spectrum recorded at 2 μs after pulse irradiation of N_2O-saturated aqueous solutions of 2×10^{-4} M *c*-(L-Met−L-Met). Figure 1A−C displays the experimental optical spectra (●) recorded at three different times after pulse irradiation of N_2O-saturated aqueous solutions of 2×10^{-4} M *c*-(L-Met−L-Met). It is apparent from the experimental spectrum in Figure 1A that the reaction between *c*-(L-Met−L-Met) and the hydroxyl radical is not a simple oxidation with only the formation of the intramolecular S∴S-bonded radical cation (**3**); other species are also formed via neighboring group participation.

A broad absorption was observed at 2 μs after the pulse in the 260−600 nm range with $\lambda_{max} = 500$ nm and with two pronounced shoulders in the spectral ranges 350−400 nm and 270−300 nm. This spectrum can be resolved into contributions from the following components (see Chart 1): the hydroxysulfuranyl radical (**1**), the intramolecular sulfur−sulfur three-electron-bonded radical cation (**3**), the intramolecular sulfur−nitrogen three-electron-bonded radical (**4**), the two α-(alkylthio)alkyl radicals (**5a**/ **5b**), and the C-centered radical located on the methionine C^{α} moiety (**7**). The sum over all component spectra with their respective yields resulted in an excellent fit (solid

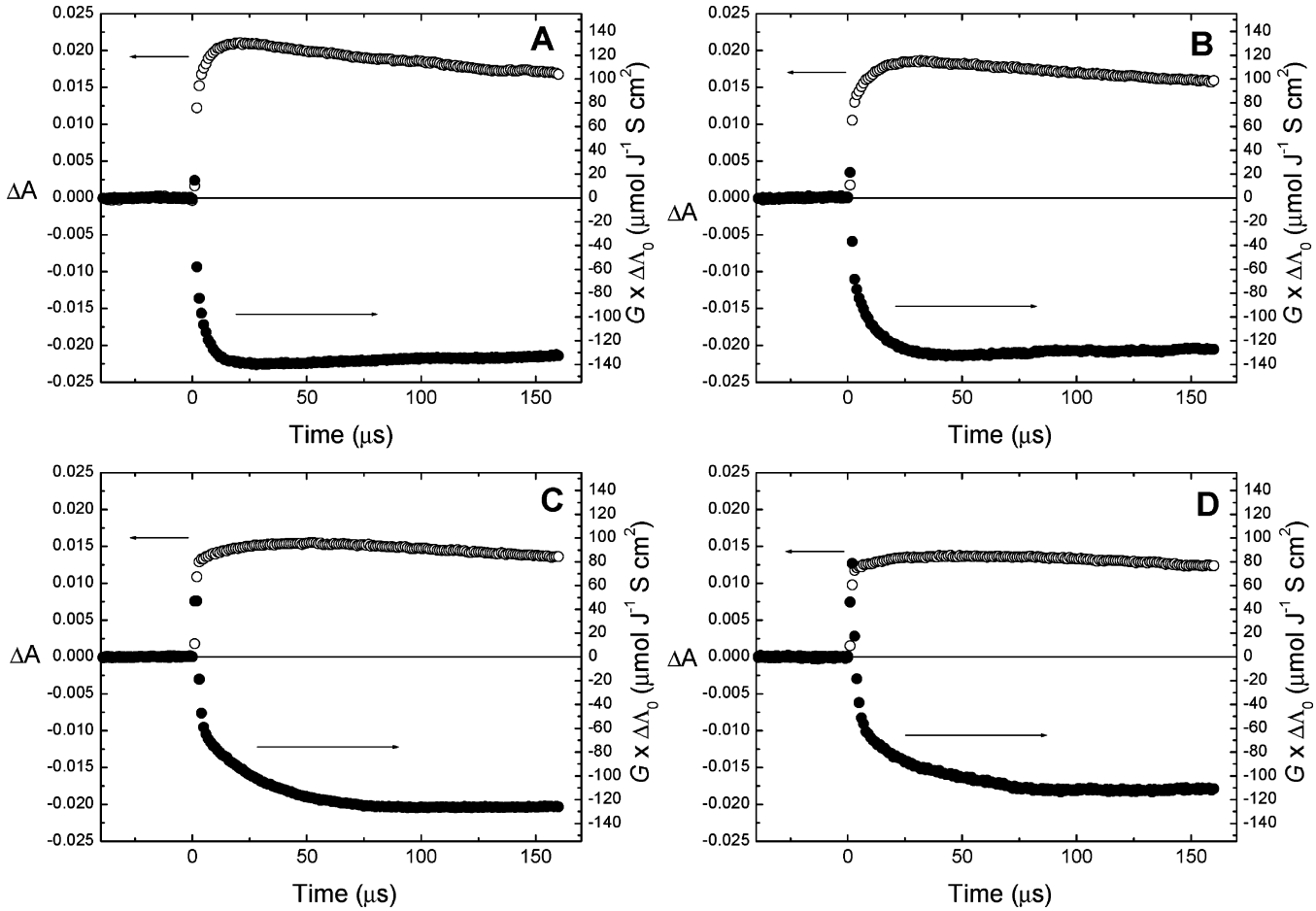

Figure 2. (A) Absorption changes at $\lambda = 500$ nm represented as (ΔA) (top traces) and equivalent conductivity changes represented as $G\Delta\Lambda$ vs time profile (bottom traces) following the •OH-induced oxidation of *c*-(L-Met−L-Met) (2×10^{-4} M) in N_2O-saturated aqueous solutions at pH values (A) 4.0, (B) 4.3, (C) 4.9, and (D) 5.3.

line) to the experimental spectrum. The G value of the radical cations **3**, $G(\mathbf{3}) = 0.27 \pm 0.001$ μmol J^{-1}, matched well with the G value of the radical ions, G(ions) $= 0.26 \pm 0.003$ μmol J^{-1}, measured by time-resolved conductivity experiments (Figure 1D). At this point, it is important to note that a reasonable spectral resolution was also achieved using the intermediates **1**, **3**, **5a**/**5b**, and the intramolecular sulfur−oxygen three-electron-bonded radical cation **6**, leaving out the sulfur−nitrogen three-electron-bonded radical **4**. However, in contrast to the previous spectral resolution, the yield of the sulfur cations $G(\mathbf{3}) + G(\mathbf{6}) = 0.48$ μmol J^{-1} does not match G(ions) $= 0.26$ μmol J^{-1} as determined by conductivity measurements.

The experimental optical spectrum recorded 15 μs after the pulse was best resolved into contributions from species **3**, **4**, **5a**/**5b**, and **7** (Figure 1B). However, the G value of the radical cations **3**, $G(\mathbf{3}) = 0.40 \pm 0.001$ μmol J^{-1} did not match the G value of the radical ions, G(ions) $= 0.45 \pm 0.01$ μmol J^{-1}, measured by time-resolved conductivity experiments (Figure 1D). Inclusion of species **6**, instead of species **4**, did not result in a satisfactory agreement between the optically and conductometrically determined yields of the radical cations (Figure 1D). Thus, inclusion both of species **3** and **4** provided the best match between G(ions) $= 0.45$ μmol J^{-1} and $G(\mathbf{3}) = 0.40$ μmol J^{-1}.

A similarly excellent spectral resolution was obtained for the experimental spectrum recorded 37.5 μs after the pulse (Figure 1C) taking into account contributions from species **3**, **5a**/**5b**, and **7**. Importantly, in contrast to the picture obtained at 15 μs after the pulse, the fit of the experimental results did not require species **4** but parallel conductivity experiments required quite a significant yield of species **6** (Figure 1D). While at this delay time after the pulse, the spectral resolution resulted in an excellent fit of the experimental spectrum, the discrepancy between G(ions) $= 0.50 \pm 0.01$ μmol J^{-1} (vide infra) and $G(\mathbf{3}) = 0.42 \pm 0.001$ μmol J^{-1} is significant and more pronounced than at 15 μs. This phenomenon of the increasing mismatch between sulfur-radical cation yields and the yields of ions with increasing time delays will be discussed later (vide infra, see Discussion).

Time-Resolved Conductivity Detection at pH 4.3. At this pH and at short time delays, less than 2 μs, conductivity measurements are more difficult to interpret quantitatively (vide supra). Hence, at these times, conductivity experiments cannot be used to help make a clear distinction between species **4** and **6** which, otherwise, have similar optical spectra. Figures 1D and 2B display conductivity versus time plots recorded at pH 4.3. They show an increasing amplitude of negative conductivity within the time range of 40 μs, with a limiting negative conductivity value reached in the time range of 40−160 μs after the pulse. This observed net decrease in equivalent conductivity can be interpreted as resulting from the stoichiometric neutralization of highly conducting protons ($\Lambda = 315$ S cm^2 equiv^{-1}; reaction in eq 7) by OH$^-$ (generated via the reaction in eq 8), with the protons being replaced by the resulting sulfide radical cations ($\Lambda = 45$ S cm^2 equiv^{-1}). These sulfide radical cations

would be the intramolecular sulfur−sulfur, three-electron-bonded cation **3** and/or the sulfur−oxygen-bonded radical cation **6**.

$$H^+ + OH^- \rightarrow H_2O \quad (7)$$

$$\mathbf{1} \rightarrow \mathbf{2} + OH^- \quad (8)$$

Thus, the overall loss of equivalent conductivity was calculated as $\Lambda = +45 - 315 = -270$ S cm^2 equiv^{-1}. The radiation-chemical yields of ions, G(ions), can be calculated from the experimental changes of equivalent conductivity at given times, e.g., $G\Delta\Lambda = -69$ μmol J^{-1} S cm^2 (2 μs), -120 μmol J^{-1} S cm^2 (15 μs), -140 μmol J^{-1} S cm^2 (37.5 μs), and -130 μmol J^{-1} S cm^2 (150 μs) (Figures 1D and 2B). Dividing these values by $\Delta\Lambda = -270$ S cm^2 equiv^{-1} gave G(ions) $= 0.26 \pm 0.003$, 0.45 ± 0.01, 0.50 ± 0.01, and 0.48 ± 0.01 μmol J^{-1} at 2, 15, 37.5, and 150 μs after the pulse, respectively. The values of G(ions) were expected to match the sum of the G(**3**) + G(**6**) for the conducting radical cations **3** and **6** (vide supra).

Spectrophotometric and Conductivity Detection at pH 4.0−5.3. Parts A−D of Figure 2 display absorption changes at $\lambda = 500$ nm (the spectral region where **3** absorbs) together with equivalent conductivity changes represented as $G\Delta\Lambda$ versus time plots recorded at pH values of 4.0, 4.3, 4.9, and 5.3, respectively. The conductivity signals show slightly decreasing amplitudes of negative conductivity with increasing pH observed at the respective time delays following the proton relaxation processes (Figure 2A−D, bottom traces). These conductivities at the times corresponding to the end of the proton relaxations were $G\Delta\Lambda = -82$ μmol J^{-1} S cm^2 (pH 4.0 at 2 μs), -69 μmol J^{-1} S cm^2 (pH 4.3 at 2 μs), -68 μmol J^{-1} S cm^2 (pH 4.9 at 6 μs), -65 μmol J^{-1} S cm^2 (pH 5.3 at 7 μs). Division of these experimental changes of $G\Delta\Lambda$ (at the end of the proton relaxations) by $\Delta\Lambda = -270$ S cm^2 equiv^{-1} gave G(ions) $= 0.30 \pm 0.01$, 0.26 ± 0.003, 0.25 ± 0.01, and 0.24 ± 0.01 μmol J^{-1} at pH values 4.0, 4.3, 4.9, and 5.3, respectively. It is important to note that the yields of intramolecular sulfur−sulfur three-electron-bonded radical cations **3** agree quite well with the total yield of ions measured by time-resolved conductometry. The radiation-chemical yields of **3** were calculated from the absorption changes (ΔA) at $\lambda = 500$ nm (Figure 2A−D, top traces), with the assumption that **3** was the only transient that absorbs at this wavelength. Thus, at the time delays from above G(**3**) $= 0.30 \pm 0.001$, 0.27 ± 0.001, 0.25 ± 0.001, and 0.25 ± 0.001 μmol J^{-1} at pH values 4.0, 4.3, 4.9, and 5.3, respectively. Therefore, we conclude that the resulting yields of **3** account, by themselves, quantitatively for the observed conductivity although their yields might be slightly overestimated.

The following features of equivalent conductivity changes ($G\Delta\Lambda$) and absorption changes (ΔA) at $\lambda = 500$ nm are important with respect to the elapsed time. Generally, the time profiles of the conductivity changes reflected the time profiles of the optical absorption changes with regard to the respective times for maximal loss of net conductivity and for maximal absorption change at $\lambda = 500$ nm. However, within the time range of 160 μs after the pulse, the maximal losses in the net conductivities $G\Delta\Lambda$ showed only a slight decrease with increasing pH, i.e., -140 μmol J^{-1} S cm^2 (pH 4.0), -136 μmol J^{-1} S cm^2 (pH 4.3), -126 μmol J^{-1} S cm^2 (pH 4.9), and -116 μmol J^{-1} S cm^2 (pH 5.3). On the other hand, the maximal net losses were reached at different times, i.e., 27.5 μs, 37.5 μs, 80 μs, and 80 μs, respectively. Division of the experimental changes of equivalent conductivity at given times gave G(ions) $= 0.52 \pm 0.01$, 0.50 ± 0.01, 0.47 ± 0.01, and 0.43 ± 0.01 μmol J^{-1} at pH values 4.0, 4.3, 4.9, and 5.3, respectively. Again, the radiation-chemical yields of **3** were calculated from the absorption changes (ΔA) at $\lambda = 500$ nm with the same assumptions as above (Figure 2A−D). At the same respective time delays, G(**3**) $= 0.43 \pm 0.001$, 0.42 ± 0.001, 0.30 ± 0.001, and 0.30 ± 0.001 μmol J^{-1} at pH values 4.0, 4.3, 4.9, and 5.3, respectively. These results show that there is a significant mismatch between the optically determined yields of **3** and the conductometrically determined yields of ions.

Concentration Profiles of Transient Formation Following $^{\bullet}$OH-Induced Oxidation of *c*-(L-Met−L-Met) at pH 4.0−5.3. Resolutions of absorption spectra at any desired time delay following the electron pulse together with total yield of ions measured by time-resolved conductometry at various pH values were performed in order to explain the mismatch between the optically determined yields of **3** and conductometrically determined yields of ions. Of particular concern was the potential contribution of the sulfur−oxygen-bonded radical cations **6** to the total yields of ions. The direct determination of G(**6**) from the experimental absorption spectra was almost impossible, even with the spectral-resolution procedure because the spectral shape of radical **6**'s absorption is almost identical to that of **4**. Figure 3A− D shows a radiation-chemical yield (G) versus time plot for the intermediates **3**, **4**, **5a/5b**, and **7** together with the total yield of ions measured by time-resolved conductometry at four pHs. The weighting of the conductivity, described above, allowed the discrimination of radicals **4** (nonconducting) and **6** (conducting).

In order to validate the optical spectral resolutions at pH 4.9 and 5.3 by comparison with concomitant changes of equivalent conductivities, the earliest time delay at which spectral resolutions were performed were at 6 and 7 μs, respectively, following pulse irradiation of N_2O-saturated aqueous solutions of 2×10^{-4} M *c*-(L-Met−L-Met). For these two pHs, at shorter time delays, conductivity measurements were more difficult to interpret quantitatively because of the slow proton equilibration (vide supra).

The total yield of all radical intermediates, $G = 0.60$ μmol J^{-1}, agrees well with the initial yield of primary radicals, $G_i(^{\bullet}OH + {}^{\bullet}H) = 0.61$ μmol J^{-1}. The apparent decay of **4** (▼) occurs with the accompanying formation of **3** (■) (Figure 3AD). On the basis of the extracted concentration profiles of the transients at various pHs, it was possible to evaluate the rate constant for radical **4** reacting with protons (Figure 4A) and also the rate constant for the formation of the radical cation **3** (Figure 4B).

Decays of **4** were fitted using the formula $G = G_0 \exp(-k_{obs}t) + G_{lim}$, where G_0 is the initial yield of **4**, G_{lim} is the final yield of **4**, and k_{obs} is the pseudo-first-order rate constant for the decay of **4**. The parameters obtained (G_0, G_{lim}, and k_{obs}) are listed in Table 1.

At this point it is worthwhile to note that the initial G_0 values of **4** do not depend on the pH and are equal to 0.27 ± 0.01 μmol J^{-1}. Interestingly, the decay rate of **4** was pH-dependent, decaying faster with increasing proton concentration (Figure 4A). From the plot of the pseudo-first-order rate constants versus proton concentration (insert in Figure 4A), the rate constant k(**4** + H$^+$) was determined to be $(2.1 \pm 0.1) \times 10^9$ M^{-1} s^{-1}.

Formations and decays of **3** were fitted using the formula $G = G_0' \exp(-k_1 t) + G_0''[\exp(-k_1 t) - \exp(-k_{obs}t)]$, where G_0' is the initial yield of **3**, G_0'' is the yield of **3** formed in the secondary process, k_1 is the pseudo-first-order rate constant for decay of **3**, and k_{obs} is the pseudo-first-order rate constant for formation of **3**. The parameters obtained (G_0', G_0'', k_1, and k_{obs}) are listed in Table 2.

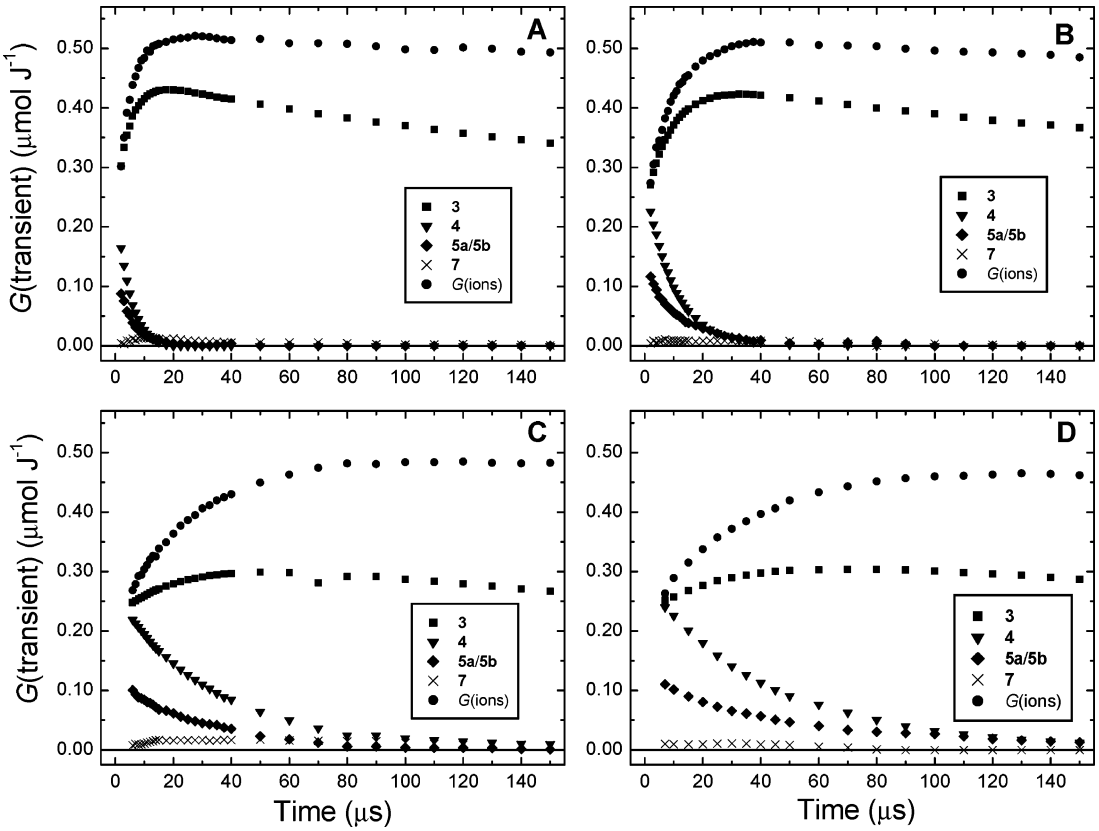

Figure 3. Radiation chemical yields vs time profiles for intermediates obtained after pulse radiolysis of N_2O-saturated aqueous solutions containing *c*-(L-Met−L-Met) (2×10^{-4} M) at pH values (A) 4.0, (B) 4.3, (C) 4.9, and (D) 5.3. Insets: explanation of symbols.

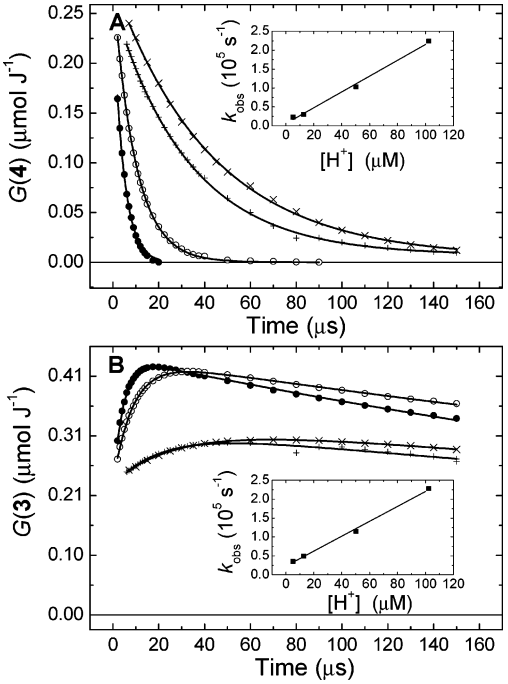

Figure 4. (A) Concentration profiles for intramolecular sulfur−nitrogen three-electron-bonded radical **4** represented as radiation chemical yields (*G*) vs time at various pHs: 4.0 (●), 4.3 (○), 4.9 (+), and 5.3 (×). Inset: dependence of k_{obs} for the decay of **4** on [H$^+$]. (B) Concentration profiles for intramolecular sulfur−sulfur three-electron-bonded radical **3** represented as radiation chemical yields (*G*) vs time at various pH values: 4.0 (●), 4.3 (○), 4.9 (+), and 5.3 (×). Inset: dependence of k_{obs} for formation of **3** on [H$^+$].

It is also worthwhile to note that the initial G_0' values of **3** did not depend on the pH and were equal to 0.23 ± 0.01 μmol J^{-1}. Interestingly, G_0'', the yield of **3**, formed in the secondary process, was pH-dependent, being lower with decreasing proton concentration. Similar to the decay rate of **4**, the formation rate of **3** was pH-dependent, forming faster with increasing proton concentration (Figure 4B). (No particular significance should be attached to the decay rates k_1 since the time range is too small to determine them with any confidence; this fitting parameter was put in only to assist in the determination of the growth rates.) From the plot of the pseudo-first-order rate constants versus proton concentration, the bimolecular rate constant *k* for formation of **3** due to the involvement of protons was determined to be $(2.0 \pm 0.1) \times 10^9$ M^{-1} s^{-1} (insert in Figure 4B).

The observed change in the pseudo-first-order rate constants for the decay of **4** was reflected in the observed change of the

TABLE 1: Fitting Parameters of the Decay of Intramolecular Sulfur−Nitrogen Three-Electron Bonded Radicals 4 at Various pHs Using the Function: $G = G_{lim} + G_0 \exp(-k_{obs}t)$

pH	G_0 (μmol J^{-1})	G_{lim} (μmol J^{-1})	k_{obs} (s^{-1})
4.0	0.26	0	2.25×10^5
4.3	0.28	0	1.05×10^5
4.9	0.25	0.005	3.00×10^4
5.3	0.27	0.005	2.30×10^4

TABLE 2: Fitting Parameters of the Decay of Intramolecular Sulfur−Sulfur Three-Electron Bonded Radical Cations 3 at Various pHs Using the Function: $G = G_0' \exp(-k_1t) + G_0''[\exp(-k_1t) - \exp(-k_{obs}t)]$

pH	G_0' (μmol J^{-1})	G_0'' (μmol J^{-1})	k_1 (s^{-1})	k_{obs} (s^{-1})
4.0	0.22	0.23	1.90×10^3	2.30×10^5
4.3	0.23	0.22	1.35×10^3	1.15×10^5
4.9	0.22	0.10	1.20×10^3	4.95×10^4
5.3	0.23	0.11	1.05×10^3	3.55×10^4

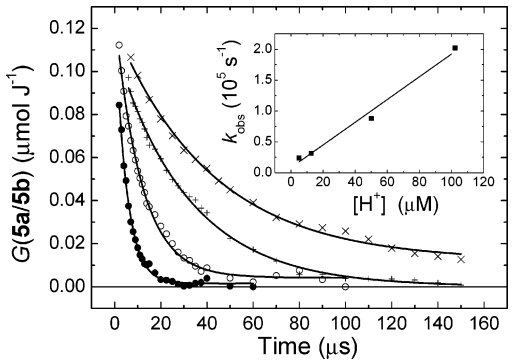

Figure 5. Concentration profiles for α-(alkylthio)alkyl radicals **5a/5b** represented as radiation chemical yields (G) vs time at various pH values: 4.0 (●), 4.3 (○), 4.9 (+), and 5.3 (×). Inset: dependence of k_{obs} for the decay of **5a/5b** on [H^+].

TABLE 3: Fitting Parameters of the Decay of α-(Alkylthio)alkyl Radicals 5a/5b at Various pHs Using the Function: $G = G_{lim} + G_0 \exp(-k_{obs}t)$

pH	G_0 (μmol J^{-1})	G_{lim} (μmol J^{-1})	k_{obs} (s^{-1})
4.0	0.13	0	2.0×10^5
4.3	0.13	0.0052	8.8×10^4
4.9	0.11	0	3.1×10^4
5.3	0.11	0.010	2.4×10^4

pseudo-first-order rate constants for the secondary formation of **3**, with these two rate constants being almost equal. This suggests that the transformation of **4** to **3** was controlled by the rate of protonation of **4**.

An excellent resolution of the experimental spectra requires inclusion of α-(alkylthio)alkyl radicals **5a/5b**. In contrast to the picture obtained in *N*-acetyl methionine amide, *N*-acetyl methionine methyl ester, and *N*-acetylated linear oligopeptides containing methionine, the radicals **5a/5b** do not show rapid formation within a few tens of microseconds,[49] and surprisingly, they decay in a pH-dependent manner over the same time domain (Figure 5).

Decays of **5a/5b** were fitted using the formula $G = G_0 \exp(-k_{obs}t) + G_{lim}$, where G_0 is the initial yield of **5a/5b**, G_{lim} is the final yield of **5a/5b**, and k_{obs} is the pseudo-first-order rate constant for decay of **5**. The parameters obtained (G_0, G_{lim}, and k_{obs}) are listed in Table 3.

The initial G_0 values of **5a/5b** did not significantly depend on the pH and were in the range of 0.11−0.13. From the plot of the pseudo-first-order rate constants versus proton concentration, the rate constant k(**5a/5b** + H^+) was determined to be $(1.85 \pm 0.15) \times 10^9$ M^{-1} s^{-1} (insert in Figure 5).

It should also be noted that the fits of the experimental transient spectra required negligible yields of **7** ($G < 0.01$ μmol J^{-1}) for any time delay shorter than 160 μs after the electron pulse at all pHs. These observations indicate that the steady-state concentration of species **7** was always low within the observed time range, i.e., 160 μs.

Theoretical Calculations

Species Derived from *c*-(L-Met−Gly). Calculations were performed on *c*-(L-Met−Gly). The calculations involve the native cyclic peptide molecule and its radicals and radical cations that were stabilized through the formation of S∴N or S∴O bonds in the cyclic peptides. This cyclic peptide served as our model of *c*-(L-Met−L-Met) to the extent that intramolecular interactions of the sulfur atom in *c*-(L-Met−L-Met), itself, are limited only to the heteroatoms (N and O) in the peptide bonds. The native peptide molecule (*c*-(L-Met−Gly)) and its radicals and radical cations, resulting from •OH-induced oxidation, were optimized and their stable structures were obtained (see part 2 of the Supporting Information). The fully relaxed gas-phase and the IEFPCM-model geometry optimization in each category resulted in several thermodynamically stable conformers.

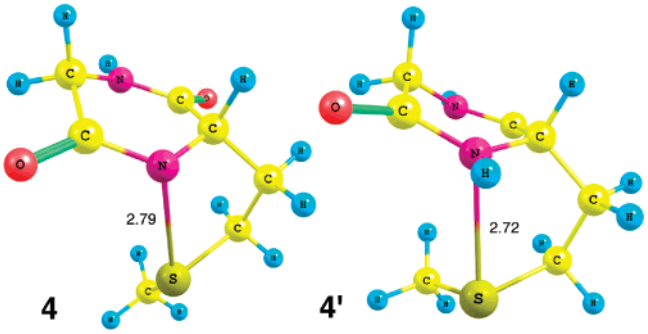

Figure 6. Representative B3LYP/6-31G(d)-optimized structures of the lowest energy conformers of the intramolecular sulfur−nitrogen three-electron-bonded radical **4** and its protonated form, intramolecular sulfur−nitrogen three-electron-bonded radical cation **4′** derived from *c*-(L-Met−Gly).

Figure 6 displays the structures and relevant geometric parameters for the lowest energy conformers of the intramolecular sulfur−nitrogen three-electron-bonded radical **4** (conformer D4 in Supporting Information, part 2) and its protonated form, the intramolecular sulfur−nitrogen three-electron-bonded radical cation (**4′**, see Scheme 2; conformer C2 in Supporting Information, part 2). The respective free energies of conformers of the native peptide and the radicals and radical cations considered in this paper are compiled as attached to their respective conformers in part 2 of the Supporting Information.

The selected primary computed energies (listed in Table S1) allow calculations of Gibbs free-energy changes for the following reactions: (i) **1** + H_3O^+ → **4′** + $2H_2O$ (overall reaction with first step being s2, Scheme 1 followed by reaction **2** → **4′**, which is not listed in the schemes), (ii) **1** → **4** + H_2O (reaction s5, Scheme 1), and (iii) **4′** + H_2O → **4** + H_3O^+ (reaction s8, Scheme 2) which will be considered below in the discussion of the mechanisms. Thus, for the above reactions, the respective changes in Gibbs free energy are equal to

$$\Delta G_9 = [\Delta G(\mathbf{4'}) + 2\Delta G(H_2O)] - [\Delta G(\mathbf{1}) + \Delta G(H_3O^+)] \quad (9)$$

$$\Delta G_{10} = [\Delta G(\mathbf{4}) + \Delta G(H_2O)] - \Delta G(\mathbf{1}) \quad (10)$$

$$\Delta G_{11} = [\Delta G(\mathbf{4}) + \Delta G(H_3O^+)] - [\Delta G(\mathbf{4'}) + \Delta G(H_2O)] \quad (11)$$

Table S1 compiles the respective changes in Gibbs free energies for the reactions in eqs 9−11 for the various combinations of conformers involved.

One should note that formation of radical cation **4′** (conformer C2 in Table S1) from radical **1** (conformers B1−B5 in Table S1) with the involvement of an external proton is a strongly exoergonic process by 111−130 kJ mol^{-1}, depending on the respective conformers of **1** involved. Similarly, formation of radical **4** (conformer D4 in Table S1) from radical **1** (conformers B1−B5 in Table S1) using an internal proton is also an exoergonic process by 44−63 kJ mol^{-1}, depending on the respective conformers of **1** involved. Finally, a critical observation that will prove to be key in the discussion of the overall mechanisms is that deprotonation of radical cation **4′**, leading

SCHEME 1

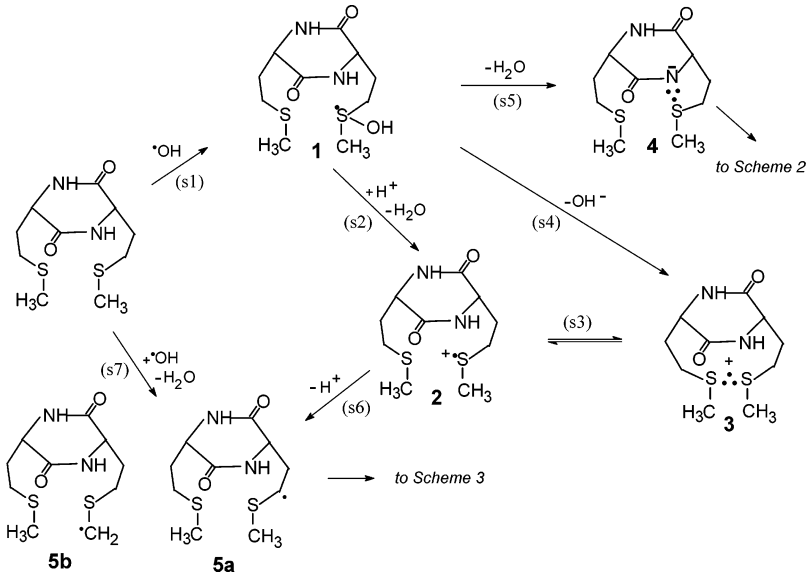

SCHEME 2

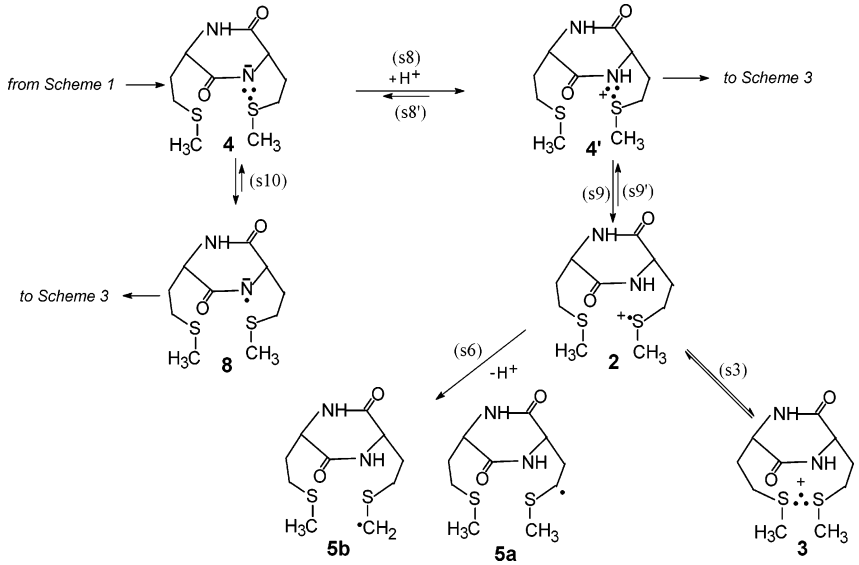

to radical **4**, is a strongly endoergonic process by 67 kJ mol^{-1} (Table S1). Two other computational methods (DFT, with BHHLYP, and MP2) confirmed the endoergonic nature of this process, 50 kJ mol^{-1} (Table S2) and 92 kJ mol^{-1} (Table S3), respectively.

Species Derived from *c*-(L-Met−L-Met). Calculations of species derived from the *c*-(L-Met−L-Met) were limited to the native cyclic peptide molecule, hydroxysulfuranyl radical **1**, and its sulfur-centered radical cations (including intramolecularly S∴S-bonded radical cations **3**). The native peptide molecule (*c*-(L-Met−L-Met)) and its radicals and radical cations, resulting from •OH-induced oxidation, were optimized and their stable structures were obtained (see part 3 of the Supporting Information). The fully relaxed gas-phase and the IEFPCM-model geometry optimization in each category resulted in several thermodynamically stable conformers. The primary computed energies (compiled as attached to their respective conformers in part 3 of Supporting Information) allow calculations of free-energy changes for the reaction **1** + H_3O^+ → **3** + $2H_2O$ (reactions s2 and s3, Scheme 1). The respective free-energy change equal to $\Delta G = [\Delta G(\mathbf{3}) + 2\Delta G(H_2O)] - [\Delta G(\mathbf{1}) + \Delta G(H_3O^+)]$ results in $\Delta G \approx -147$ kJ mol^{-1}. This process is more exoergonic by 84 kJ mol^{-1} than the formation process of radical **4** from radical **1** using an internal proton.

Free Energies of Deprotonation of the Amide Functionality. The free energies of deprotonation of the amide functionality were calculated for *c*-(Gly−Gly), *c*-(L-Ala−L-Ala), and *N*-methylacetamide taking primary computed energies of the native molecules and the respective anions (see part 4 of the Supporting Information). The calculated energies show that deprotonation of the amide functionality in all peptides represented by the reaction in eq 12 is a very unfavorable process (endoergonic by 155−184 kJ mol^{-1}). However, it can be noted that depro-

$$RH + H_2O \rightarrow R^- + H_3O^+ \qquad (12)$$

tonation of the amide functionality in the diketopiperazine ring in *c*-(Gly−Gly) and *c*-(L-Ala−L-Ala) is thermodynamically more favorable by approximately 29−40 kJ mol^{-1} (applying the Gaussian-3/DFT theory) than the analogous process in both the cis and trans conformations of the amide functionality of *N*-methylacetamide (taken as the simplest model of open-chain peptides). The observed Gibbs free-energy advantage of the cyclic peptides over the linear amide seems to be due to relief

in the conformational strain of the diketopiperazine ring accompanying deprotonation.

Discussion

Similarity and Difference of *c*-(L-Met−L-Met) to Linear N-Acetylated Peptides Containing Methionines. Considerable mechanistic information has been accumulated about the primary reactions of hydroxyl radicals with small organic thioethers and methionine-containing peptides.[19,25,28,40,52,62,83−98] The initial reaction of •OH with *c*-(L-Met−L-Met) was identical to those with linear L-Met-containing peptides in that it led to the formation of the hydroxysulfuranyl radical **1** (reaction s1, Scheme 1).[49]

However, significant differences exist with respect to the subsequent reactions. On a short time scale (<4 μs), specifically at pH 4, the hydroxysulfuranyl radical of linear N-acetylated model peptides containing L-Met (such as the simple structure *N*-acetylmethionine amide) decomposed into intermolecular S−S and intramolecular S−O three-electron-bonded radical cations, where the sulfur−oxygen bond was formed with the peptide bond.[17,49] This mechanism was corroborated by a simultaneous change in equivalent conductivity, which paralleled the formation of both species. At higher pH values, the S−O-bonded radical cations deprotonated at the peptide-bond amide nitrogen followed by a rearrangement to yield "neutral" S−N-bonded radicals. The latter converted, in part, to capto-datively stabilized radicals centered at the Met C_α carbon.[49]

Hydroxysulfuranyl radicals **1** of *c*-(L-Met−L-Met) also decomposed into intramolecularly S−S-bonded radical cations **3** (either via reactions s2 and s3 or directly via reaction s4, Scheme 1). Since there was no influence of pH on the primary yields of **3** (see Table 2), this suggests that reaction s4 (Scheme 1) represents an important pathway for the formation of **3**.

However, in stark contrast to the linear N-acetylated peptides containing L-Met,[49] approximately 55% of radical **1** converted immediately into the neutral S−N-bonded species **4** through elimination of water (reaction s5, Scheme 1). In this concerted process, elimination of OH^- in the form of water involved a simultaneous N-deprotonation from the amide nitrogen in **1** followed by formation of **4** in the form of a thermodynamically favorable five-membered ring.

Rationalization for the Formation of Neutral S−N-Bonded Species 4. Calculated energies clearly indicate that the formation of **4** via reaction s5 (Scheme 1) is thermodynamically favorable (Table S1, middle section). The quantitative analysis of the spectral and conductivity data allows us to conclude that the S−N-bonded radical cation **4′** was not a likely intermediate since its formation (reaction s2, Scheme 1 and reaction s9′, Scheme 2) would be also associated with a net decrease in conductivity. Therefore, we believe the S−N-bonded radical **4**, absorbing in the 380−420 nm region, has a deprotonated form at one of its amide functions.

This mechanism resembles the proposed reaction of hydroxysulfuranyl radicals of free L-Met, where intramolecular proton transfer from the N-terminal $-NH_3^+$ group leads to the elimination of water.[40] The direct formation of **4** in *c*-(L-Met−L-Met), but the absence of an analogous mechanism in linear N-acetylated peptides containing L-Met, suggests the occurrence of an analogous proton transfer from the amide of the cyclic peptide. That is, the heterolytic cleavage of the peptide amide bond in *c*-(L-Met−L-Met) is significantly more favorable, corroborated by the lower amide pK_a values of cyclic vs linear peptides.[99,100] This was also confirmed by our calculations (where deprotonation of the cyclic amide was 39.8 kJ mol^{-1} more favorable compared to the linear model CH_3CONH_2). Importantly, theoretical calculations argue against the formation of radical **4** via hydroxide elimination from **1** to yield the monomeric radical cation **2** (reaction s4, Scheme 1) followed by cyclization to **4′** (reaction s9′ in Scheme 2) and deprotonation to **4** (reaction s8′ in Scheme 2). This follows from consideration of the Gibbs free energy change for the deprotonation of **4′** to **4** which is approximately +67 kJ mol^{-1}, that is, represents a strongly endoergonic reaction (Table S1 see C2 → D4 in the bottom section).

pH-Dependence of Secondary Formation of S−S-Bonded Radical Cations. At 2 μs after pulse irradiation of *c*-(L-Met−L-Met), the initial hydroxysulfuranyl radical **1** was completely decomposed into radical cation **3** and radical **4**. The small yield of α-(alkylthio)alkyl radicals **5a**/**5b** was likely due to direct H-abstraction from *c*-(L-Met−L-Met) by •OH/H• radicals. The subsequent reactions over a longer time scale distinguished the cyclic peptide even more from N-acetylated peptides containing L-Met. To rationalize these mechanistic differences, we will first summarize a few key observations important for the ensuing discussion: (a) The neutral S−N-bonded radicals **4** decayed in a proton-catalyzed reaction to yield only additional radical cations **3** (reactions s8, s9, and s3 in Scheme 2). Contrary to N-acetylated peptides containing L-Met, S−O-bonded radical cations **6** (see Chart 1) were not formed. The efficiency of conversion of **4** into **3** appeared to be pH-dependent. At pH 4, radical **4** was generated with $G = 0.26$ μmol J^{-1} (after correction for its fast decay, see Table 1), and after the decomposition of **4**, the yield of **3** was increased by a difference $\Delta G = 0.23$ μmol J^{-1}, i.e., from $G = 0.22$ μmol J^{-1} to $G = 0.45$ μmol J^{-1} (Table 2). At pH 4.3, an initial yield of **4** of $G = 0.28$ μmol J^{-1} (after correction for its fast decay, see Table 1) decomposed with the formation of additional **3** with $\Delta G = 0.22$ μmol J^{-1}. At pH values 4.9 and 5.3, such quantitative comparison shows that conversion of **4** into **3** occurred with lower efficiencies: $\Delta G(\mathbf{4}) = 0.25$ μmol J^{-1} → $\Delta G(\mathbf{3}) = 0.10$ μmol J^{-1} and $\Delta G(\mathbf{4}) = 0.27$ μmol J^{-1} → $\Delta G(\mathbf{3}) = 0.11$ μmol J^{-1}, respectively (Tables 1 and 2). It is worthwhile to note that the yields, $G(\mathbf{4})$, that are not accounted for in the corresponding formation yields of $G(\mathbf{3})$, increase with pH. The discrepancies in these G values are equal to 0.04, 0.06, 0.15, and 0.17 μmol J^{-1} for pH values 4.0, 4.3, 4.9, and 5.3, respectively. These numbers were computed from the respective G values in Table 1 (G_0) and Table 2 (G_0'').

Explaining Discrepancy between Yields of Ions Measured from Spectroscopy vs Conductivity. Importantly, for all pH values, the total radiation-chemical yield of radical cations **3** ($G' + G_0''$ in Table 2) is not sufficient to explain a much higher yield of ions calculated based on a change in the conductivity signal, especially at longer times, assuming the replacement of a proton with an organic ion of lower equivalent conductivity, ($G_{ions}\Delta\Lambda$) (Figure 3A−D). Hence, besides the protonation of **4** (reaction s8, Scheme 2), leading to the additional yields of **3**, another pathway, or pathways, must exist, which does not lead to radical cations **3**.

This apparent mismatch between ionic yields from spectroscopy and conductivity might be associated with the consumption of protons, which could accompany further protonation of the species present. In the following, we consider two alternate pathways that can consume protons and, together, account for this mismatch. One involves a competitive route for the disappearance of **4**, and the other involves a pH-dependent channel for the decay of **5a**/**5b**.

The extent of the amount of **4** that can disappear by the first alternate channel can be computed. The respective yields $G(\mathbf{4})$

SCHEME 3

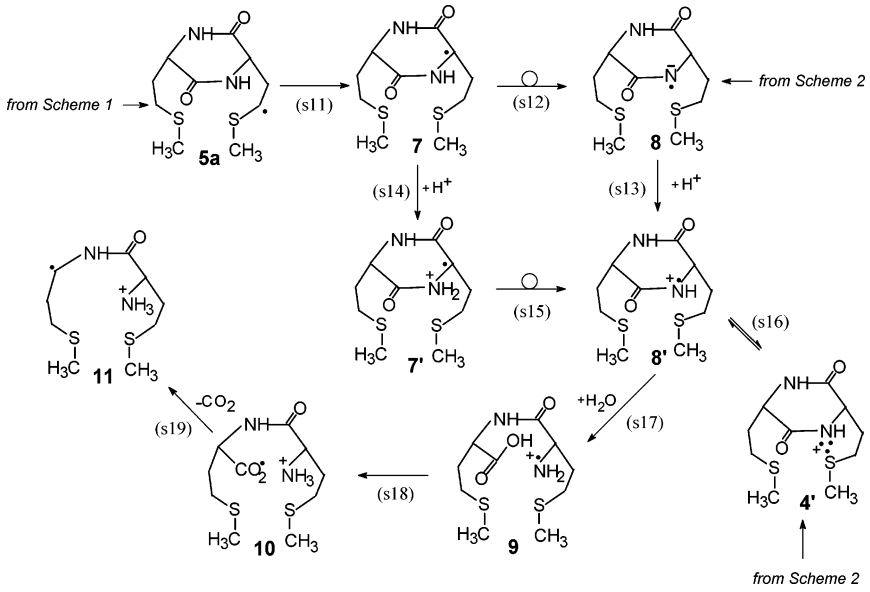

that were not accounted for in the formation yields of G(**3**) were equal to 0.04, 0.06, 0.15, and 0.17 μmol J^{-1} at pH values 4.0, 4.3, 4.9, and 5.3, respectively (vide supra). This observation could be rationalized if another reaction pathway competes with the formation of **3** from **4**. For instance, reaction s10 (Scheme 2) might compete efficiently with reaction s8 (Scheme 2), leading to the N-centered radical **8** that undergoes protonation (reaction s13, Scheme 3), and this would, then, contribute to the net conductivity changes. In other words, the yield of this apparent discrepancy might be taken as a measure of the yield of N-centered radical cations **8′** formed via reactions s10 (Scheme 2) and s13 (Scheme 3). However, these considerations only rationalize to some extent the apparent discrepancy between the yield of ions obtained from time-resolved conductivity measurements and the yield of ions obtained from spectral resolutions. From Figure 3A−D, these discrepancies can be seen to be equal to 1.50, 1.20, 2.10, and 1.70 for pH values 4.0, 4.3, 4.9, and 5.3, respectively. Therefore, discrepancies in yields of 1.15, 0.6, 0.65, and 0.1 have yet to be accounted for. This mismatch, large in particular for pH 4.0, might be associated with the consumption of protons, which could accompany further protonation of another species present.

The second pathway proposed is related to the decomposition of the α-(alkylthio) radicals **5a** and **5b**. In fact, the behavior of these two species represents perhaps the most significant difference between *c*-(L-Met−L-Met) and analogous radicals in linear peptides containing methionine. In these linear peptides, most sulfur-centered radicals/radical cations will ultimately convert into relatively stable (100 μs time scale) α-(alkylthio)-alkyl radicals like **5a** and **5b**.[49] In contrast, in *c*-(L-Met−L-Met), these α-(alkylthio)alkyl radicals decompose in a proton-catalyzed reaction within tens of microseconds. Quantitatively, the decomposition of **5a**/**5b** accounts approximately for the larger mismatch between the total yield of ions and the yield of **3**, specifically at pH 4.

An important feature of the unknown species that undergo protonation is that they cannot absorb significantly between 300 and 600 nm. We tentatively propose that radicals **5a** and **5b** reacted via the mechanism depicted in Scheme 3. On the basis of theoretical considerations, the 1,3-H-shift in **5a** (displayed in reaction s11, Scheme 3) and the 1,5-H-shift in **5b** should be exoergonic. Both of these H-atom shifts lead to the C-centered radical **7**. Radical **7** was observed under our experimental conditions but with a very low G value of <0.01 μmol J^{-1}, indicating that it must undergo further transformations if formed. Reaction s12 to yield the nitrogen-centered radical **8** is proposed based on analogous pathways discussed for carbon-centered radicals of amino acids.[101] Protonation of both **7** (reaction s14, Scheme 3) and **8** (reaction s13, Scheme 3) to yield **7′** and **8′** is likely endoergonic. However, hydrolysis of **8′** to **9** (reaction s17, Scheme 3) followed by electron/proton transfer (reaction s18, Scheme 3) and decarboxylation (reaction s19, Scheme 3)) may lead to an overall exoergonic process, ultimately yielding the stabilized radical **11**. The spectral properties of **11**-type radicals are known ($\lambda_{max} < 300$ nm),[96] and the overall process requires the uptake of one proton equivalent per equivalent of **11**. Hence, the formation of **11** could rationalize all the experimental observations.

Conclusions

In the current paper, we have provided further experimental proof that the one-electron oxidation by •OH radicals of a simple cyclic dipeptide containing two methionine residues leads to efficient formation of the Met(S∴N) radicals. This is a strongly competitive process to the formation of Met(S∴S)$^+$ radical cations in spite of the close proximity of sulfur atoms located in the side chains of methionine residues and the close proximity of sulfur atoms and oxygen atoms located in the peptide bonds. Moreover, we have shown that formation of Met(S∴N) radicals involves the hydrogen atom of the peptide bond. These Met(S∴N) radicals decay via two different pH-dependent mechanisms. At low pH, Met(S∴N) radicals convert efficiently into Met(S∴S)$^+$ radical cations that are stable for hundreds of microseconds. Our current findings may be useful for the interpretation of data obtained with proteins containing multiple methionine residues since they underline the importance of the stabilization of Met(S$^{+\bullet}$) by heteroatoms in peptide bonds, a phenomenon that might be of general importance during oxidation of proteins.

Very recent studies of calmodulin (CaM−Ca$_4$, wild type) by pulse radiolysis have supported the first experimental evidence for the formation of Met(S$^{+\bullet}$) which complexes to amide groups in adjacent peptide bonds.[102] The nine Met residues in calmodulin find themselves in a variety of local environments, so the stabilization of Met(S$^{+\bullet}$) can be realized in various ways

depending on local structure. For example, two pairs of Met residues are adjacent (i.e., Met^{71}/Met^{72} and Met^{144}/Met^{145}). On the other hand, the individual Met residues have proximity to different nucleophilic groups located either in peptide bonds or in side groups of amino acid residues.

Under conditions where significant amounts of sulfide radical cation complexes and superoxide are formed simultaneously, reactions of the sulfide radical cation−nucleophile complexes, $Met(S\therefore S)^+$ and $Met(S\therefore N)^+$, with superoxide radical anions ($O_2^{\bullet-}$) and O_2 represent an efficient sulfoxide- and azasulfonium-forming processes, respectively.[103−105] From a biological point of view, it is important to note that the reaction of $O_2^{\bullet-}$ with the sulfide radical cation−nucleophile complexes $Met(S\therefore S)^+$ and $Met(S\therefore N)^+$ proceeds faster[103] than the reaction of $O_2^{\bullet-}$ with superoxide dismutase.[106,107] These reactions might represent a potential source for sulfoxide formation in proteins containing methionine residues, e.g., for the intracellular protein calmodulin.[108,109]

Acknowledgment. Dedicated to the memory of Professor Dave Armstrong. This work described herein was supported by the NATO Travel Grant PST CLG 977628, Research Training Network SULFRAD (Grant HPRN-CT-2002-00184), Polish Ministry of Scientific Research Grant 3 T09A 066 26, Office of Basic Energy Sciences of the U.S. Department of Energy, and ESF under COST Action P9 RADAM (K.B. and D.P.). The computation was performed employing the computing resources of the Interdisciplinary Centre for Mathematical and Computation Modeling, Warsaw University, Poland (Grant G24-13). This paper is the Document No. NDRL-4636 from the Notre Dame Radiation Laboratory.

Supporting Information Available: Details of the computation, Cartesian coordinates (in Å) for structures, and the total energies of the species calculated. This material is available free of charge via the Internet at http://pubs.acs.org.

References and Notes

(1) Schöneich, C. *Biochim. Biophys. Acta* **2005**, *1703*, 111−119.
(2) Fourré, I.; Bergès, J. *J. Phys. Chem. A* **2004**, *108*, 898−906.
(3) Huang, M. L.; Rauk, A. *J. Phys. Chem. A* **2004**, *108*, 6222−6230.
(4) Brunelle, P.; Rauk, A. *J. Phys. Chem. A* **2004**, *108*, 11032−11041.
(5) Schöneich, C. *Arch. Biochem. Biophys.* **2002**, *397*, 370−376.
(6) Rauk, A.; Armstrong, D. A.; Fairlie, D. P. *J. Am. Chem. Soc.* **2000**, *122*, 9761−9767.
(7) Glass, R. S. *Top. Curr. Chem.* **1999**, *205*, 1−87.
(8) Pogocki, D.; Serdiuk, K.; Schöneich, C. *J. Phys. Chem. A* **2003**, *107*, 7032−7042.
(9) Pogocki, D.; Schöneich, C. *J. Org. Chem.* **2002**, *67*, 1526−1535.
(10) Braïda, B.; Hazebroucq, S.; Hiberty, P. C. *J. Am. Chem. Soc.* **2002**, *124*, 2371−2378.
(11) Carmichael, I. *Nukleonika* **2000**, *45*, 11−17.
(12) Carmichael, I. *Acta Chem. Scand.* **1997**, *51*, 567−571.
(13) Clark, T. Sulfur-Centered Three-Electron Bonded Radical Species. In *Sulfur-Centered Reactive Intermediates in Chemistry and Biology*; Chatgilialoglu, C., Asmus, K.-D., Eds.; Plenum Press: New York 1990; Vol. 197, pp 13−18.
(14) Asmus, K.-D. Heteroatom-Centered Free Radicals: Some Selected Contributions by Radiation Chemistry. In *Radiation Chemistry: Present Status and Future Trends*; Jonah, C., Madhava Rao, B. S., Eds.; Elsevier Science: Amsterdam, The Netherlands, 2001; pp 341−393.
(15) Asmus, K.-D. *Nukleonika* **2000**, *45*, 3−10.
(16) Hug, G. L.; Bobrowski, K.; Kozubek, H.; Marciniak, B. *Photochem. Photobiol.* **2000**, *72*, 1−9.
(17) Schöneich, C.; Pogocki, D.; Wisniowski, P.; Hug, G. L.; Bobrowski, K. *J. Am. Chem. Soc.* **2000**, *122*, 10224−10225.
(18) Asmus, K.-D.; Bonifačić, M. Sulfur-Centered Reactive Intermediates as Studied by Radiation Chemical and Complementary Techniques. In *S-Centered Radicals*; Alfassi, Z. B., Ed.; John Wiley & Sons Ltd.: Chichester, U.K., 1999; pp 141−191.
(19) Bobrowski, K.; Pogocki, D.; Schöneich, C. *J. Phys. Chem. A* **1998**, *102*, 10512−10521.
(20) Hug, G. L.; Bobrowski, K.; Kozubek, H.; Marciniak, B. *Photochem. Photobiol.* **1998**, *68*, 785−796.
(21) Bobrowski, K.; Hug, G. L.; Marciniak, B.; Miller, B. L.; Schöneich, C. *J. Am. Chem. Soc.* **1997**, *119*, 8000−8011.
(22) Chaudhri, S. A.; Mohan, H.; Anklam, E.; Asmus, K.-D. *J. Chem. Soc., Perkin Trans. 2* **1996**, 383−390.
(23) Champagne, M. H.; Mullins, M. W.; Colson, A.-O.; Sevilla, M. D. *J. Phys. Chem.* **1991**, *95*, 6487−6493.
(24) Hungerbuehler, H.; Guha, S. N.; Asmus, K.-D. *J. Chem. Soc., Chem. Commun.* **1991**, 999−1000.
(25) Steffen, L. K.; Glass, R. S.; Sabahi, M.; Wilson, G. S.; Schöneich, C.; Mahling, S.; Asmus, K.-D. *J. Am. Chem. Soc.* **1991**, *113*, 2141−2145.
(26) Anklam, E.; Asmus, K.-D.; Mohan, H. *J. Phys. Org. Chem.* **1990**, *3*, 17−22.
(27) Mohan, H. *J. Chem. Soc., Perkin Trans. 2* **1990**, 1821−1824.
(28) Bobrowski, K.; Holcman, J. *J. Phys. Chem.* **1989**, *93*, 6381−6387.
(29) Anklam, E.; Mohan, H.; Asmus, K.-D. *J. Chem. Soc., Perkin Trans. 2* **1988**, 1297−1302.
(30) Anklam, E.; Mohan, H.; Asmus, K.-D. *Helv. Chim. Acta* **1987**, *70*, 2110−2117.
(31) Anklam, E.; Mohan, H.; Asmus, K.-D. *J. Chem. Soc., Chem. Commun.* **1987**, 629−630.
(32) Bobrowski, K.; Holcman, J. *Int. J. Radiat. Biol. Relat. Stud. Phys., Chem. Med.* **1987**, *52*, 139−144.
(33) Mahling, S.; Asmus, K.-D.; Glass, R. S.; Hojjatie, M.; Wilson, G. S. *J. Org. Chem.* **1987**, *52*, 3717−3724.
(34) Mohan, H.; Asmus, K.-D. *J. Am. Chem. Soc.* **1987**, *109*, 4745−4746.
(35) Bobrowski, K.; Holcman, J. *Radiat. Phys. Chem.* **1986**, *28*, 555.
(36) Asmus, K.-D.; Göbl, M.; Hiller, K.-O.; Mahling, S.; Mönig, J. *J. Chem. Soc., Perkin Trans. 2* **1985**, 641−646.
(37) Mönig, J.; Göbl, M.; Asmus, K.-D. *J. Chem. Soc., Perkin Trans. 2* **1985**, 647−651.
(38) Asmus, K.-D.; Bahnemann, D.; Fischer, C.-H.; Veltwisch, D. *J. Am. Chem. Soc.* **1979**, *101*, 5322−5329.
(39) Bonifačić, M.; Asmus, K.-D. *J. Org. Chem.* **1986**, *51*, 1216−1222.
(40) Hiller, K.-O.; Masloch, B.; Göbl, M.; Asmus, K.-D. *J. Am. Chem. Soc.* **1981**, *103*, 2734−2743.
(41) Davies, M. *Biochim. Biophys. Acta* **2005**, *1703*, 93−109.
(42) Stadtman, E. R.; Van Remmen, H.; Richardson, A.; Wehr, N. B.; Levine, R. L. *Biochim. Biophys. Acta* **2005**, *1703*, 135−140.
(43) Levine, R. L.; Berlett, B. S.; Moskovitz, J.; Mosoni, L.; Stadtman, E. L. *Mech. Ageing Dev.* **1999**, *107*, 323−332.
(44) Levine, R. L.; Mosoni, L.; Berlett, B. S.; Stadtman, E. R. *Proc. Natl. Acad. Sci. U.S.A.* **1996**, *93*, 15036−15040.
(45) Martin, G. M. *Exp. Gerontol.* **2000**, *35*, 439−443.
(46) Glasser, C. B.; Yamin, G.; Uversky, V. N.; Fink, A. L. *Biochim. Biophys. Acta* **2005**, *1703*, 157−169.
(47) Butterfield, D. A.; Kimball-Boyd, D. *Biochim. Biophys. Acta* **2005**, *1703*, 149−156.
(48) Zahn, R.; Liu, A.; Luhrs, T.; Riek, R.; Von Schroetter, C.; Lopez Garcia, F.; Billeter, M.; Calzolai, L.; Wider, G.; Wuhtrich, K. *Proc. Natl. Acad. Sci. U.S.A.* **2000**, *97*, 145−150.
(49) Schöneich, C.; Pogocki, D.; Hug, G. L.; Bobrowski, K. *J. Am. Chem. Soc.* **2003**, *125*, 13700−13713.
(50) Glass, R. S.; Petsom, A.; Hojjatie, M.; Coleman, B. R.; Duchek, J. R.; Klug, J.; Wilson, G. S. *J. Am. Chem. Soc.* **1988**, *110*, 4772−4778.
(51) Kadlčik, V.; Sicard-Roselli, C.; Mattioli, T. A.; Kodiček, M.; Houee-Levin, C. *Free Radical Biol. Med.* **2004**, *37*, 881−891.
(52) Holcman, J.; Bobrowski, K.; Schöneich, C.; Asmus, K.-D. *Radiat. Phys. Chem.* **1991**, *37*, 473−478.
(53) von Sonntag, C. *The Chemical Basis of Radiation Biology*; Taylor and Francis: New York, 1987.
(54) Janata, E.; Schuler, R. H. *J. Phys. Chem.* **1982**, *86*, 2078−2084.
(55) Schuler, R. H.; Hartzell, A. L.; Behar, B. *J. Phys. Chem.* **1981**, *85*, 192−199.
(56) Hug, G. L.; Wang, Y.; Schöneich, C.; Jiang, P.-Y.; Fessenden, R. W. *Radiat. Phys. Chem.* **1999**, *54*, 559−566.
(57) Janata, E. *Radiat. Phys. Chem.* **1982**, *19*, 17−21.
(58) Asmus, K.-D. *Int. J. Radiat. Phys. Chem.* **1972**, *4*, 417−437.
(59) Veltwisch, D.; Janata, E.; Asmus, K.-D. *J. Chem. Soc., Perkin Trans. 2* **1980**, 146−153.
(60) Bevington, P. R. *Data Reduction and Error Analysis for the Physical Sciences*; McGraw-Hill: New York, 1969.
(61) Marciniak, B.; Bobrowski, K.; Hug, G. L. *J. Phys. Chem.* **1993**, *97*, 11937−11943.
(62) Schöneich, C.; Bobrowski, K. *J. Am. Chem. Soc.* **1993**, *115*, 6538−6547.
(63) Pogocki, D. M. Investigation of Radical Processes Induced by Hydroxyl Radical in Amino Acids and Peptides Containing Thioether Group. Ph.D. Thesis, Institute of Nuclear Chemistry and Technology, Warsaw, Poland, 1996.

(64) Hiller, K.-O.; Asmus, K.-D. *Int. J. Radiat. Biol. Relat. Stud. Phys., Chem. Med.* **1981**, *40*, 597−604.
(65) Mieden, O. J.; von Sonntag, C. *Z. Naturforscher* **1989**, *44b*, 959−974.
(66) Wisniowski, P.; Hug, G. L. *Decom2006*, 2006.
(67) Frisch, M. J.; Trucks, G. W.; Schlegel, H. B.; Scuseria, G. E.; Robb, M. A.; Cheeseman, J. R.; Montgomery, J. A., Jr.; Vreven, T.; Kudin, K. N.; Burant, J. C.; Millam, J. M.; Iyengar, S. S.; Tomasi, J.; Barone, V.; Mennucci, B.; Cossi, M.; Scalmani, G.; Rega, N.; Petersson, G. A.; Nakatsuji, H.; Hada, M.; Ehara, M.; Toyota, K.; Fukuda, R.; Hasegawa, J.; Ishida, M.; Nakajima, T.; Honda, Y.; Kitao, O.; Nakai, H.; Klene, M.; Li, X.; Knox, J. E.; Hratchian, H. P.; Cross, J. B.; Bakken, V.; Adamo, C.; Jaramillo, J.; Gomperts, R.; Stratmann, R. E.; Yazyev, O.; Austin, A. J.; Cammi, R.; Pomelli, C.; Ochterski, J. W.; Ayala, P. Y.; Morokuma, K.; Voth, G. A.; Salvador, P.; Dannenberg, J. J.; Zakrzewski, V. G.; Dapprich, S.; Daniels, A. D.; Strain, M. C.; Farkas, O.; Malick, D. K.; Rabuck, A. D.; Raghavachari, K.; Foresman, J. B.; Ortiz, J. V.; Cui, Q.; Baboul, A. G.; Clifford, S.; Cioslowski, J.; Stefanov, B. B.; Liu, G.; Liashenko, A.; Piskorz, P.; Komaromi, I.; Martin, R. L.; Fox, D. J.; Keith, T.; Al-Laham, M. A.; Peng, C. Y.; Nanayakkara, A.; Challacombe, M.; Gill, P. M. W.; Johnson, B.; Chen, W.; Wong, M. W.; Gonzalez, C.; Pople, J. A. *Gaussian 03*, revision B.03; Gaussian, Inc.: Pittsburgh, PA, 2003.
(68) Becke, A. D. *J. Chem. Phys.* **1993**, *98*, 5648−5652.
(69) Korzeniowska-Sobczuk, A.; Hug, G. L.; Carmichael, I.; Bobrowski, K. *J. Phys. Chem. A* **2002**, *106*, 9251−9260.
(70) Maity, D. K. *J. Am. Chem. Soc.* **2002**, *124*, 8321−8328.
(71) Braïda, B.; Thogersen, L.; Wu, W.; Hiberty, P. C. *J. Am. Chem. Soc.* **2002**, *124*, 11781−11790.
(72) McKee, M. L. *J. Phys. Chem. A* **2003**, *107*, 6819−6827.
(73) Young, D. C. *Computational Chemistry. A Practical Guide for Applying Techniques to Real World Problems*; John Wiley & Sons Ltd: New York, 2001.
(74) Jensen, F. *Introduction to Computational Chemistry*; John Wiley & Sons Ltd: Chichester, U.K., 1999.
(75) Davidson, E. R.; Feller, D. *Chem. Rev.* **1986**, *86*, 681−696.
(76) Cances, E.; Mennucci, B.; Tomasi, J. *J. Chem. Phys.* **1998**, *109*, 260−266.
(77) Cossi, M.; Barone, V.; Mennucci, B.; Tomasi, J. *Chem. Phys. Lett.* **1998**, *286*, 253−260.
(78) Cances, E.; Mennucci, B.; Tomasi, J. *J. Chem. Phys.* **1997**, *107*, 3032−3041.
(79) Baboul, A. G.; Curtiss, L. A.; Redfern, P. C.; Raghavachari, K. *J. Chem. Phys.* **1999**, *110*, 7650−7657.
(80) Curtiss, L. A.; Redfern, P. C.; Raghavachari, K.; Rassolov, V.; Pople, J. A. *J. Chem. Phys.* **1999**, *110*, 4703−4709.
(81) Ando, S.; Fujigaya, T.; Ueda, M. *Jpn. J. Appl. Phys.* **2002**, *41*, L105−L108.
(82) Casida, M. E.; Jamorski, C.; Casida, K. C.; Salahub, D. R. *J. Chem. Phys.* **1998**, *108*, 4439−4449.
(83) Varmenot, N.; Bergès, J.; Abedinzadeh, Z.; Scemama, A.; Strzelczak, G.; Bobrowski, K. *J. Phys. Chem. A* **2004**, *108*, 6331−6346.
(84) Mohan, H.; Mittal, J. P. *J. Phys. Chem. A* **2002**, *106*, 6574−6580.
(85) Varmenot, N.; Remita, S.; Abedinzadeh, Z.; Wisniowski, P.; Strzelczak, G.; Bobrowski, K. *J. Phys. Chem. A* **2001**, *105*, 6867−6875.
(86) Bobrowski, K.; Hug, G. L.; Marciniak, B.; Schöneich, C.; Wisniowski, P. *Res. Chem. Intermed.* **1999**, *25*, 285−297.
(87) Gawandi, V. B.; Mohan, H.; Mittal, J. P. *Chem. Phys. Lett.* **1999**, *314*, 451−458.
(88) Gawandi, V. B.; Mohan, H.; Mittal, J. P. *J. Chem. Soc., Perkin Trans. 2* **1999**, 1425−1432.
(89) Bobrowski, K.; Schöneich, C. *Radiat. Phys. Chem.* **1996**, *47*, 507−510.
(90) Schöneich, C.; Zhao, F.; Madden, K. P.; Bobrowski, K. *J. Am. Chem. Soc.* **1994**, *116*, 4641−4652.
(91) Bobrowski, K.; Pogocki, D.; Schöneich, C. *J. Phys. Chem.* **1993**, *97*, 13677−13684.
(92) Schöneich, C.; Aced, A.; Asmus, K.-D. *J. Am. Chem. Soc.* **1993**, *115*, 11376−11383.
(93) Bobrowski, K.; Schöneich, C. *J. Chem. Soc., Chem. Commun.* **1993**, 795−797.
(94) Bobrowski, K.; Schöneich, C.; Holcman, J.; Asmus, K.-D. *J. Chem. Soc., Perkin Trans. 2* **1991**, 353−362.
(95) Bobrowski, K.; Schöneich, C.; Holcman, J.; Asmus, K.-D. *J. Chem. Soc., Perkin Trans. 2* **1991**, 975−980.
(96) Hiller, K.-O.; Asmus, K.-D. *J. Phys. Chem.* **1983**, *87*, 3682−3688.
(97) Bonifačić, M.; Schäfer, K.; Möckel, H.; Asmus, K.-D. *J. Phys. Chem.* **1975**, *79*, 1496.
(98) Bonifačić, M.; Möckel, H.; Bahnemann, D.; Asmus, K.-D. *J. Chem. Soc., Perkin Trans. 2* **1975**, 675−685.
(99) Forsyth, W. R.; Robertson, A. D. *J. Am. Chem. Soc.* **1996**, *118*, 2694−2698.
(100) Molday, R. S.; Kallen, R. G. *J. Am. Chem. Soc.* **1972**, *94*, 6739−6745.
(101) Bonifačić, M.; Stefanič, I.; Hug, G. L.; Armstrong, D. A.; Asmus, K.-D. *J. Am. Chem. Soc.* **1998**, *120*, 9930−9940.
(102) Nauser, T.; Jacoby, M.; Koppenol, W. H.; Squier, T. C.; Schöneich, C. *Chem. Commun.* **2005**, 587−589.
(103) Bonifačić, M.; Hug, G. L.; Schöneich, C. *J. Phys. Chem. A* **2000**, *104*, 1240−1245.
(104) Miller, B. L.; Williams, T. D.; Schöneich, C. *J. Am. Chem. Soc.* **1996**, *118*, 11014−11025.
(105) Miller, B. L.; Kuczera, K.; Schöneich, C. *J. Am. Chem. Soc.* **1998**, *120*, 3345−3356.
(106) Rotilio, G.; Bray, R. C.; Fielden, E. M. *Biochim. Biophys. Acta* **1972**, *268*, 605−609.
(107) Klug, D.; Rabani, J.; Fridovich, I. *J. Biol. Chem.* **1972**, *247*, 4839−4842.
(108) Sharov, V. S.; Schöneich, C. *Free Radical Biol. Med.* **2000**, *29*, 986−994.
(109) Michaelis, M. L.; Bigelow, D. J.; Schöneich, C.; Williams, T. D.; Ramonda, L.; Yin, Hühmer, A. F. R.; Yao, Y.; Gao, J.; Squier, T. C. *Life Sci.* **1996**, *59*, 405−412.